Using polarimetry to detect and characterize Jupiter-like extrasolar planets

Stam, D.M.; Hovenier, J.W.; Waters, L.B.F.M.

DOI
10.1051/0004-6361:20041578
Publication date
2004

Published in
Astronomy & Astrophysics

A&A 428, 663–672 (2004)
DOI: 10.1051/0004-6361:20041578

Astronomy & Astrophysics

Using polarimetry to detect and characterize Jupiter-like extrasolar planets

D. M. Stam[1], J. W. Hovenier[1], and L. B. F. M. Waters[1,2]

[1] Astronomical Institute "Anton Pannekoek", University of Amsterdam, Kruislaan 403, 1098 SJ Amsterdam, The Netherlands
e-mail: dstam@science.uva.nl
[2] Instituut voor Sterrenkunde, K.U. Leuven, Celestijnenlaan 200B, 3001 Heverlee, Belgium

Received 14 April 2004 / Accepted 9 August 2004

Abstract. Using numerical simulations of flux and polarization spectra of visible to near-infrared starlight reflected by Jupiter-like extrasolar planets, we show that polarimetry can be used both for the detection and for the characterization of extrasolar planets. Polarimetry is valuable for detection because direct, unscattered starlight is generally unpolarized, while starlight that has been reflected by a planet will generally be polarized. Polarimetry is valuable for planet characterization because the degree of polarization of starlight that has been reflected by a planet depends strongly on the composition and structure of the planetary atmosphere.

Key words. techniques: polarimetric – stars: planetary systems – polarization

1. Introduction

Since the discovery of a planet around 51Peg (Mayor & Queloz 1995), the number of known extrasolar planets around solar-type stars has increased to more than 120 today. These extrasolar planets have been discovered using indirect detection methods, in which not radiation from the planet itself, but the planet's influence on the star is observed. Given the currently used detection methods, it is not surprising that the vast majority of the extrasolar planets discovered so far have minimum masses that are typical of giant, gaseous planets, and orbital radii of at most a few astronomical units. Apart from some orbital parameters and a lower mass limit, little is known about the planets' physical characteristics. A notable exception is the planet around HD 209458, that can be observed transiting its star (see Charbonneau et al. 2000, and references therein). Such a transit not only allows the observer to estimate the planetary size and mass, but it also gives information on upper atmospheric constituents (Charbonneau et al. 2002; Vidal-Majar et al. 2003, 2004).

Although transits can provide information on extrasolar planetary atmospheres, as in the case of HD 209458b, they are not suited for the characterization (i.e. the derivation of chemical compositions, sizes, and spatial distributions of atmospheric constituents, such as cloud particles) of such atmospheres in general; not only because they probe merely the upper atmospheric layers, but also because the chances of a planet with e.g. a Jupiter-like orbit (about 5.2 AU) being observable in transit are less than 0.1% (this chance can roughly be described as R/D, with R the stellar radius and D the planet's orbital radius). Clearly, the characterization of an extrasolar planet's atmosphere requires observing the thermal radiation the planet emits and/or the stellar light it reflects directly. Besides making the characterization of atmospheres possible, direct observations of planetary radiation will also enable the detection of extrasolar planets that are not easily found with the currently used indirect detection methods, such as planets that are not very massive and/or in wide orbits.

Direct observations of extrasolar planets are not yet available: they are extremely challenging because the faint signal of an extrasolar planet is easily lost in the bright stellar glare. In this paper, we discuss the use of polarimetry both for the enhancement of the contrast between a planet and its parent star, thus facilitating the detection of an extrasolar planet, and for the characterization of the planet. Polarimetry can help planet detection because, integrated over the stellar disk, direct starlight can be considered to be unpolarized (Kemp et al. 1987), while starlight that has been reflected by the planet will generally be polarized. Polarimetry can be used for planet characterization because the degree of polarization of the reflected starlight depends strongly on the composition and structure of the planetary atmosphere. This is well-known from remote-sensing of solar system planetary atmospheres, in particular Venus (Hansen & Hovenier 1974) and the Earth (see e.g. Hansen & Travis 1974, and references therein).

Because of their sizes and because many of them are already known to exist thanks to indirect detection methods, the first extrasolar planets to be detected directly will most likely

be giant, gaseous planets (Extrasolar Giant Planets or EGPs). In this paper, we use numerical simulations of starlight that is reflected by Jupiter-like EGPs to illustrate several advantages of polarimetry for extrasolar planet detection and characterization. Numerically simulated polarization signals of extrasolar giant planets have been presented earlier by Seager et al. (2000), Saar & Seager (2003), and Hough & Lucas (2003). These authors, however, considered so-called close-in EGPs (CEGPs), that have orbital radii $\leq$0.05 AU, and, consequently, very high temperatures ($\sim$1000 K). Because of the small orbital radii, it will not be possible to spatially resolve the (polarized) light reflected by such a close-in EGP from the (unpolarized) direct light of its parent star. As a result, the degree of polarization that one can measure for such an unresolved planetary system is expected to be very small ($\sim 10^{-5}$) (see Seager et al. 2000; Saar & Seager 2003; Hough & Lucas 2003).

Because P is a relative measure, it can be determined very accurately: the accuracy of sophisticated polarimeters is of the order of 10^{-5} (Povel 1995), and more sensitive (better than 10^{-6}) polarimeters are being built with the detection of extrasolar planets in mind (see Hough & Lucas 2003). Although such sensitivities are imperative for planet detection in unresolved planetary systems, the mere detection of an EGP in a Jupiter-like orbit that can be spatially resolved from its star can be performed with a less accurate polarimeter. However, when observing such EGPs, the use of an accurate polarimeter is strongly recommended, because, as we will illustrate in this paper, polarimetry is a valuable tool not only for detecting EGPs, but also for the characterization of their atmospheres (i.e. the derivation of chemical compositions, sizes, and spatial distributions of atmospheric constituents, such as cloud particles),

In this paper, we concentrate on polarization signals of EGPs at Jupiter-like distances (several astronomical units) from their star. In the near-future, such planets may be spatially resolved from their star, for example, from space, or from the ground in combination with adaptive optics systems to correct for atmospheric turbulence. With a spatially resolved planetary system, in which the polarized planetary light can be observed without dilution by the unpolarized stellar light, it will be possible to measure high degrees of polarization, as we will show here. We will discuss the dependence of the polarization of the planetary light on the planetary atmosphere, on the geometry, and, in particular, on the wavelength. This spectral dependence is important for determining optimal instrumental wavelength regions for planet detection and/or planet characterization.

An example of an instrument for direct detection of EGPs that combines polarimetry, spectroscopy, and adaptive optics, is CHEOPS (CHaracterizing Exoplanets by Opto-infrared Polarimetry and Spectroscopy) (Feldt et al. 2003) that has been proposed to ESO for use on the VLT. CHEOPS will use the well-established and highly accurate (10^{-5}) Zürich imaging polarimeter (ZIMPOL) (Povel et al. 1990; Povel 1995) for detection and characterization of extrasolar planets. With CHEOPS/ZIMPOL a (suspected) planetary system will be imaged in two perpendicular polarization directions. Unpolarized sources, like the star, will be equally bright in these two images, whereas a polarized source, like a planet, will show up in the difference between the images. CHEOPS' polarimetry is planned to be performed in the near-infrared, across the I-band.

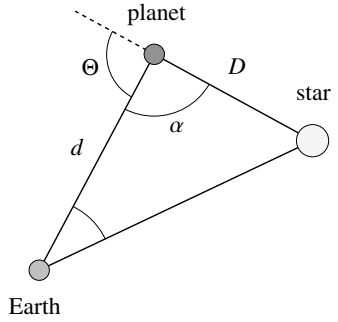

Fig. 1. Distances and angles involved in observing an extrasolar planet: α is the phase angle, Θ ($=\pi - \alpha$) is the scattering angle ($0 \leq \Theta \leq \pi$), D is the distance between the star and the planet, and d is the distance between the planet and the Earth. Note that in our numerical simulations of starlight reflected by the planet, we assume $d \gg r$ and $D \gg R$, with r the radius of the planet, and R the stellar radius.

In Sect. 2, we introduce the Stokes vector description of planetary radiation and polarization. In Sect. 3, we describe the radiative transfer algorithm and the atmospheric models of the Jupiter-like EGPs we use in the numerical simulations. Section 4 contains the numerically simulated total and polarized fluxes of the EGPs, and in Sect. 5 we discuss and summarize the advantages of polarimetry for extrasolar planet detection and characterization.

2. Planetary radiation

2.1. Stokes vectors and polarization

The flux (irradiance) and state of polarization of planetary radiation with wavelength λ can be described by a Stokes (column) vector $\boldsymbol{F}$ (see Hovenier & van der Mee 1983)

$$\boldsymbol{F}(\lambda, \alpha) = [F(\lambda, \alpha), Q(\lambda, \alpha), U(\lambda, \alpha), V(\lambda, \alpha)], \quad (1)$$

with α the planetary phase angle, i.e. the angle between the star and the observer as seen from the center of the planet (see Fig. 1). Here, the Stokes parameter F describes the total, Q and U the linearly polarized, and V the circularly polarized flux. All Stokes parameters in Eq. (1) have the dimension W m^{-2} m^{-1}.

Stokes parameters Q and U are defined with respect to a reference plane. We chose our reference plane through the centers of the star, the planet, and the observer. This plane is referred to as the planetary scattering plane. Stokes vectors can be transformed from this reference plane to another, e.g. the optical plane of a polarimeter, using the following rotation matrix (see Hovenier & van der Mee 1983)

$$\boldsymbol{L}(\beta) = \begin{bmatrix} 1 & 0 & 0 & 0 \\ 0 & \cos 2\beta & \sin 2\beta & 0 \\ 0 & -\sin 2\beta & \cos 2\beta & 0 \\ 0 & 0 & 0 & 1 \end{bmatrix}. \quad (2)$$

Angle β is the angle between the two reference planes, measured rotating in the anti-clockwise direction from the original to the new reference plane when looking towards the observer.

The degree of polarization P of the radiation described by Stokes vector $\boldsymbol{F}$ (see Eq. (1)), is defined as

$$P(\lambda,\alpha) = \frac{\sqrt{Q^2(\lambda,\alpha) + U^2(\lambda,\alpha) + V^2(\lambda,\alpha)}}{F(\lambda,\alpha)}. \quad (3)$$

Assuming that the planet is mirror-symmetric with respect to the reference plane, Stokes parameters U and V are zero when integrated over the planetary disk. In that case, the degree of polarization of the reflected light can simply be defined as

$$P(\lambda,\alpha) = -Q(\lambda,\alpha)/F(\lambda,\alpha). \quad (4)$$

In Eq. (4), we have included the minus sign to add information about the direction of polarization: for $P > 0$ ($P < 0$), the light is polarized perpendicular (parallel) to the reference plane.

2.2. Reflected starlight

Given a spherical extrasolar planet with radius r, the planetary radiation (see Eq. (1)) with wavelength λ that has been reflected by the planet and that arrives at a distance d (with $d \gg r$) can be described by

$$\boldsymbol{F}(\lambda,\alpha) = \frac{r^2}{d^2}\,\frac{R^2}{D^2}\,\frac{1}{4}\boldsymbol{S}(\lambda,\alpha)\,\pi\boldsymbol{B}_0(\lambda). \quad (5)$$

In Eq. (5), R is the stellar radius, and D the distance between the star and the planet (with $D \gg R$). Figure 1 shows the phase angle and the distances appearing in Eq. (5). Note that, analogous to the scattering of light by a particle, $180^\circ - \alpha = \Theta$, with Θ the so-called total scattering angle. Furthermore in Eq. (5), $\boldsymbol{S}$ is the planetary scattering matrix, and $\boldsymbol{B}_0$ represents the Stokes (column) vector $[B_0, 0, 0, 0] = B_0\,[1, 0, 0, 0]$, with πB_0 the stellar surface flux (in W m^{-2} m^{-1}). Integrated over the stellar disk, this flux can be considered to be unpolarized (Kemp et al. 1987), hence the use of the unit column vector. The starlight is assumed to be unidirectional ($D \gg R$) when it arrives at the planet.

The planetary scattering matrix $\boldsymbol{S}$ describes the light that has been scattered within the planetary atmosphere and that is reflected towards the observer. Because for years to come, extrasolar planets will be observable as point sources only (once they are directly observable), $\boldsymbol{S}$ describes the reflected starlight integrated over the illuminated and visible part of the planetary disk. Matrix $\boldsymbol{S}$ will generally depend strongly on the wavelength λ of the reflected light, through the composition and structure of the planetary atmosphere and the optical properties of the atmospheric constituents like gases, aerosol, and cloud particles (see Sect. 3), and on the planetary phase angle α, which determines which fraction of the illuminated side of the planet can actually be observed (see Sect. 4).

Using the planetary scattering plane as the reference plane, and assuming a planet that is mirror-symmetric with respect to this reference plane, the planetary scattering matrix $\boldsymbol{S}$ is given by (see Hovenier 1969)

$$\boldsymbol{S}(\lambda,\alpha) = \begin{bmatrix} a_1(\lambda,\alpha) & b_1(\lambda,\alpha) & 0 & 0 \\ b_1(\lambda,\alpha) & a_2(\lambda,\alpha) & 0 & 0 \\ 0 & 0 & a_3(\lambda,\alpha) & b_2(\lambda,\alpha) \\ 0 & 0 & -b_2(\lambda,\alpha) & a_4(\lambda,\alpha) \end{bmatrix}. \quad (6)$$

With unpolarized incident starlight, the only elements of $\boldsymbol{S}$ that are needed to calculate the Stokes vector $\boldsymbol{F}$ of the light that is reflected by the planet are a_1 and b_1 (cf. Eq. (5)). Starlight that has been diffracted in the planetary atmosphere, and that might be observed when $\alpha = 180^\circ$ (in the case of a transiting extrasolar planet), is not included in $\boldsymbol{S}$.

Matrix $\boldsymbol{S}$ is normalized so that the average of the planetary phase function, which is represented by matrix element a_1, over all directions equals the planet's Bond (or spherical) albedo A_B, i.e.

$$\frac{1}{4\pi}\int_{4\pi} a_1(\lambda,\alpha)\,\mathrm{d}\omega = \frac{1}{2}\int_0^\pi a_1(\lambda,\alpha)\,\sin\alpha\,\mathrm{d}\alpha \equiv A_\mathrm{B}(\lambda), \quad (7)$$

where $\mathrm{d}\omega$ is an element of solid angle. The Bond albedo is the fraction of the irradiance of the incident starlight that is reflected by the planet in all directions. The planetary Bond albedo plays an important role in determining a planet's energy balance, because $1 - A_\mathrm{B}$ indicates how much stellar light is being absorbed by the planet.

For observers, the geometric albedo of a planet is more interesting than the Bond albedo, because it is a measure of the brightness of a planet. The geometric albedo A_G of a planet is defined as the ratio of the flux that is reflected by the planet at opposition (when $\alpha = 0^\circ$) to the flux reflected by a Lambertian surface (i.e. a surface that reflects all incoming radiation isotropically and completely depolarized) that receives the same incoming irradiance and that subtends the same solid angle (i.e. $\pi r^2/d^2$) on the sky. Thus,

$$A_\mathrm{G}(\lambda) = \frac{F(\lambda,0^\circ)}{B_0(\lambda)}\,\frac{D^2}{R^2}\,\frac{d^2}{\pi r^2} = \frac{1}{4}\,a_1(\lambda,0^\circ). \quad (8)$$

Note that the ratio of the Bond albedo to the geometric albedo is the so-called phase integral. Of course, to derive the absolute brightness of a planet, knowing A_G is not enough; proper values of r, d, R, D, and B_0 (see Eq. (5)) should also be available.

2.3. Thermally emitted radiation

Equation 5 describes the starlight that is reflected by the planet. Planetary radiation, however, not only consists of reflected starlight, but also of thermal radiation that is emitted by the planet. This thermal radiation is generally emitted at (near-) infrared wavelengths, and it will be unpolarized, in particular when integrated over the planetary disk. The degree of polarization of the reflected plus the thermal planetary radiation thus equals (cf. Eq. (4))

$$P(\lambda,\alpha) = -\frac{Q_\mathrm{reflected}(\lambda,\alpha)}{F_\mathrm{reflected}(\lambda,\alpha) + F_\mathrm{thermal}(\lambda,\alpha)}, \quad (9)$$

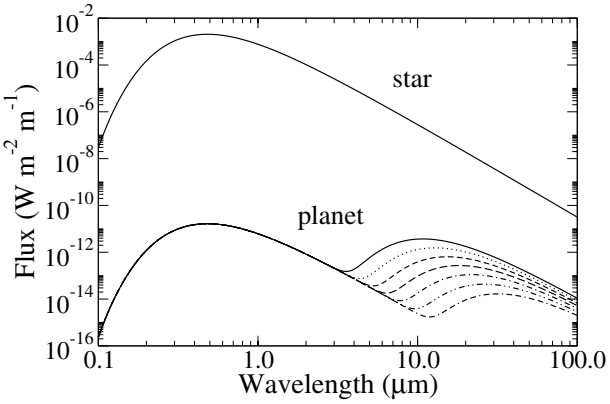

Fig. 2. The flux of a solar-type star (upper solid line) (with an effective temperature of 6000 K, and a radius of 700 000 km) at 5 pc, and the planetary flux (lower lines) of a Jupiter-like planet (with a radius of 70 000 km, and a geometric albedo of 1.0) at 5.2 AU from its star, with an age of 0.125 (solid line), 0.25, 0.5, 1.0, 2.0, 4.0, and 8.0 (dot-dash-dash line) Gyrs. The corresponding effective temperatures of the planet are respectively 268.8 (solid line), 225.6, 189.3, 159.4, 133.2, 110.4, and 91.2 K (dot-dash-dash line) (the age – temperature relations have been taken from Burrows et al. 2003). The star and planet are assumed to radiate like black bodies, and spectral features, e.g. due to absorbing gases and/or absorbing and scattering atmospheric particles, are ignored.

with $F_{\rm reflected}$ and $Q_{\rm reflected}$ given by Eq. (5). The contribution of the thermally emitted flux to the total planetary flux, and thus to the decrease of the degree of polarization P of the planetary radiation, depends strongly on the temperature of the planet.

Figure 2 shows, schematically, the flux of a solar-type star and the total planetary flux ($F_{\rm reflected} + F_{\rm thermal}$) of a Jupiter-like planet at various ages (see Burrows et al. 2003). The planet's temperature is assumed to be solely determined by the planet's age; any temperature increase due to absorption of stellar radiation is neglected. This is a reasonable assumption for a planet in a not-to-close orbit around its star, like the Jupiter-like planets we consider in this paper (remember that planets that do heat up significantly because of the absorption of stellar radiation, the so-called "roasters", will be too close to their star to be spatially resolvable). Furthermore, in Fig. 2, the star and the planet are assumed to radiate like perfect black-bodies; spectral features due to e.g. absorbing gases and/or scattering and absorbing atmospheric particles have been omitted. The phase angle α of the planet is 0°, and the planet's (wavelength independent) geometric albedo $A_{\rm G}$ is 1.0. Assuming unpolarized incoming stellar light, the flux that is reflected by the planet (in Fig. 2) is then given by (cf. Eqs. (5) and (8))

$$F(\lambda, 0^\circ) = \frac{r^2}{d^2}\,\frac{R^2}{D^2}\,\frac{1}{4}a_1(\lambda, 0^\circ)\,\pi B_0(\lambda) = \frac{r^2}{d^2}\,\frac{R^2}{D^2}\,\pi B_0(\lambda). \qquad (10)$$

The solar-type star has an effective temperature of 6000 K, and a radius R of 700 000 km. The planet has a radius r of 70 000 km, and orbits its star at a distance D of 5.2 AU. The planetary system is located at a distance d of 5 pc from the observer.

In Fig. 2, the two contributions to the planetary radiation can easily be distinguished: at the shortest wavelengths, the planetary spectrum is dominated by reflected stellar radiation, and at the longest wavelengths, by the planet's thermal radiation. For very hot planets or, for example, brown dwarfs, the thermally emitted radiation will limit the use of polarimetry to visible wavelengths (up to about 0.8 μm for a planet at 1000 K). As can be derived from the spacing of the lines in Fig. 2, Jupiter-like planets cool down relatively rapidly. The wavelength region available for polarimetry thus increases relatively rapidly towards the infrared. For a 4×10^9 years old Jupiter-like planet, reflected radiation will dominate the planetary radiation, and hence the degree of polarization of the planetary radiation, for wavelengths up to about 6.0 μm.

In Fig. 2, the planetary geometric albedo $A_{\rm G}$ was set equal to 1. With this (wavelength independent) value of $A_{\rm G}$, the (wavelength independent) ratio of the reflected stellar flux to the direct stellar flux in Fig. 2 is 0.8×10^{-8}. In reality, this ratio, the albedo and, more generally, the planetary scattering matrix $\boldsymbol{S}$, depend on the composition and structure of the planetary atmosphere, the wavelength λ, and the planetary phase angle α ($A_{\rm G}$ is phase angle independent since it has been defined for $\alpha = 0^\circ$). In this paper, we will calculate $\boldsymbol{S}$, and from that, F and P, for Jupiter-like extrasolar planets from visible to near-infrared wavelengths, in particular from 0.4 to 1.0 μm. According to Fig. 2, we can safely ignore thermally emitted planetary radiation across this wavelength region.

3. Radiative transfer calculations

3.1. Calculating the planetary scattering matrix S

The first step towards calculating $\boldsymbol{S}$ is the modeling of planetary atmospheres as stacks of locally plane-parallel, horizontally homogeneous layers, containing gaseous molecules, and, optionally, aerosol particles. A model atmosphere is bounded below by a black surface (i.e. all the light that escapes the atmosphere at the bottom is assumed to be absorbed).

Directions in the plane-parallel model atmosphere are specified by the cosine of the angle with the downward vertical, $\mu = \cos\theta$, and the azimuthal angle, ϕ. The azimuthal angle is measured from an arbitrary plane and clockwise when looking upward. The direction of the incident starlight is denoted by (μ_0, ϕ_0), and that of the light reflected towards the observer by (μ, ϕ). Since we assume horizontally homogeneous planetary atmospheres, only the azimuthal difference $\phi - \phi_0$ is relevant.

Given a plane-parallel model atmosphere, the second step towards calculating $\boldsymbol{S}$, is the computation of the local reflection matrix $\boldsymbol{R}$ for various combinations of (μ_0, ϕ_0) and (μ, ϕ). For this, we use an efficient adding-doubling radiative transfer algorithm (van de Hulst 1980) that fully includes multiple scattering and polarization (de Haan et al. 1987). For each planetary phase angle α, the various local reflection matrices are integrated over the illuminated and visible part of the planetary disk to obtain the planetary reflection matrix $\boldsymbol{S}$. Details of the computation of the planetary scattering matrix will be given in Stam et al. (in preparation).

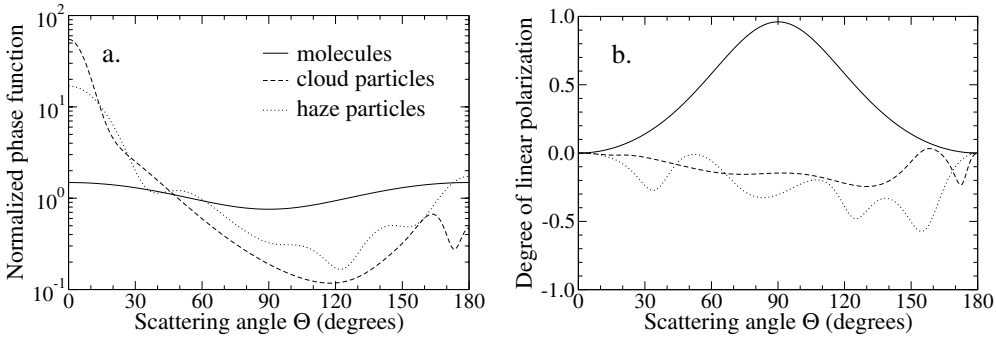

Fig. 3. The phase functions and the degree of linear polarization of light singly scattered by gaseous molecules (solid lines), the cloud particles (dashed lines), and the haze particles (dotted lines) at a wavelength $\lambda = 0.7\ \mu$m as functions of the scattering angle Θ (in degrees) (when $\Theta = 180°$, the light is scattered in the backward direction). The phase functions are normalized such that the average over all directions equals unity.

3.2. The model atmospheres

The adding-doubling radiative transfer calculations for the local reflection matrices $\boldsymbol{R}$ require us to specify for each atmospheric layer and for each wavelength: the optical thickness, the single scattering albedo, and the scattering matrix of the mixture of gaseous molecules and aerosol particles in the layer (see Stam et al. 1999).

The molecular optical thickness of an atmospheric layer depends on the ambient pressure and temperature. For this paper, we use model atmospheres consisting of 38 layers and having a Jupiter-like atmospheric pressure and temperature profile. The ambient pressure ranges from 1.0×10^{-4} bars at the top to 5.623 bars at the bottom of our model atmospheres (Lindal 1992, supplemented from 1.0 to 5.623 bars by data from West et al. 1986). Across the wavelength region of our interest (from 0.4 to 1.0 μm), methane (CH_4) is the main absorbing gas in a Jupiter-like atmosphere. We assume an atmospheric mixing ratio of CH_4 of 0.18%, like on Jupiter, and adopt the absorption cross-sections of Karkoschka (1994).

In this paper, we will present results of numerical simulations for three types of planetary model atmospheres: model 1 contains only gaseous molecules (the "clear atmosphere"), model 2 is identical to model 1 except for a tropospheric cloud layer (the "low cloud atmosphere"), and model 3 is identical to model 2 except for a stratospheric haze layer (the "high haze atmosphere"). The cloud and haze particles are homogeneous, spherical particles distributed in size according to the standard distribution of Hansen & Travis (1974). For the cloud particles, the effective radius, $r_{\rm eff}$, is taken equal to 1.0 μm and the effective variance, $v_{\rm eff}$, is 0.1. For the haze particles, $r_{\rm eff} = 0.5\ \mu$m and $v_{\rm eff} = 0.01$ (Sromovsky & Fry 2002). The refractive index of the cloud particles is 1.42, which is typical for NH_3 ice at 0.7 μm (Martonchik et al. 1984). For the refractive index of the haze particles we use 1.66 (following Sromovsky & Fry 2002).

The scattering of the gaseous molecules is described by anisotropic Rayleigh scattering, using the depolarization factor of H_2, the major constituent of a Jupiter-like atmosphere, i.e. 0.02 (see Hansen & Travis 1974). The wavelength dependent extinction cross-section, single scattering albedo, and scattering matrix of the cloud and haze particles are calculated using Mie-theory (van de Hulst 1957; de Rooij & van der Stap 1984). Figure 3a shows the phase function and Fig. 3b the degree of linear polarization P (see Eq. (4)) for incoming unpolarized light with $\lambda = 0.7\ \mu$m that has been singly scattered by, respectively, the gaseous molecules, the cloud, and the haze particles. Here, $P > 0$ ($P < 0$) indicates scattered light that is polarized perpendicular (parallel) to the scattering plane (i.e. the plane containing the incoming as well as the scattered light). The wiggles in the curves pertaining to the haze particles are due to the narrowness of the size distribution (see Hansen & Travis 1974). Figure 3b clearly shows the strong polarizing capabilities of gaseous molecules, in particular for scattering angles Θ around 90°.

Note that the scattering matrix elements of the cloud and haze particles will be wavelength dependent, whereas those of the gaseous molecules are not (ignoring the slight wavelength dependence of the depolarization factor).

The molecular scattering optical thickness of the model atmospheres decreases from 21.47 at 0.4 μm to 0.51 at 1.0 μm. The tropospheric cloud (models 2 and 3) is located in the atmospheric layers between 5.623 and 1.0 bars. Its (scattering) optical thickness is chosen to be equal to 6.0 at 0.7 μm (the cloud optical thickness of each layer is chosen proportional to the molecular scattering optical thickness of the layer). With the size distribution of the cloud particles as described above, the cloud's (scattering) optical thickness increases smoothly from 5.45 at 0.4 μm to 7.34 at 1.0 μm. The stratospheric haze (model 3) is located in the atmospheric layers between 0.133 and 0.1 bars, with a (scattering) optical thickness of 0.25 at 0.7 μm (Sromovsky & Fry 2002). The haze optical thickness varies from 0.23 at 0.4 μm to 0.35 at 1.0 μm.

As we know from observations of Jupiter in our own Solar System, the atmosphere of a Jupiter-like EGP will undoubtedly be much more complex than the model atmospheres considered in this paper: there might be latitudinal bands consisting of various cloud layers composed of numerous types of cloud particles (see e.g. Sromovsky & Fry (2002) and references therein). Our simple model atmospheres, however, suffice to illustrate both the advantages of polarimetry for the detection of EGPs

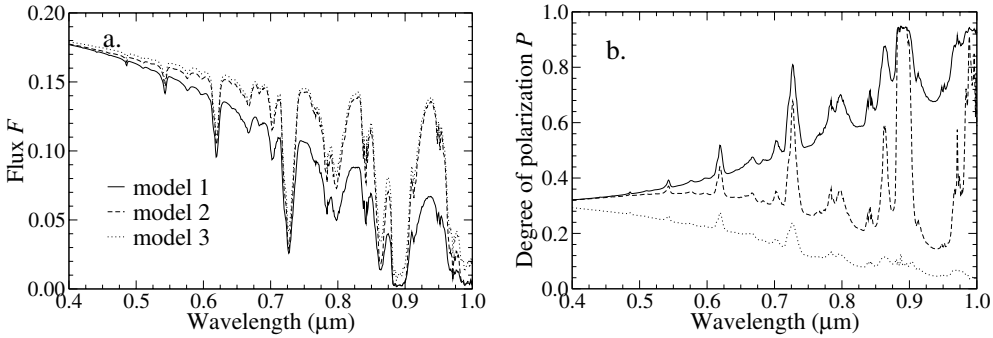

Fig. 4. The flux F and degree of polarization P of starlight reflected by three Jupiter-like EGPs for $\alpha = 90°$. Planetary model atmosphere 1 (solid lines) contains only molecules, model 2 (dashed lines) is similar to model 1, except for a tropospheric cloud layer, and model 3 (dotted lines) is similar to model 2, except for a stratospheric haze layer.

and the sensitivity of the degree of polarization of the reflected stellar radiation to the structure and composition of the planetary model atmosphere.

4. Results

4.1. Flux and polarization as functions of wavelength

Figure 4 shows spectra of the reflected flux F and degree of polarization P for the 3 model atmospheres and a planetary phase angle α of 90°. These spectra have been calculated at the same 1-nm intervals at which the CH_4 absorption cross-sections have been given (Karkoschka 1994). In order to present general results in Fig. 4, we have set $\pi B_0 r^2 R^2/(d^2 D^2)$ (see Eq. (5)) equal to one. In fact, Fig. 4a thus shows $\frac{1}{4}a_1(\lambda, 90°)$, with a_1 the (1,1)-element of the planetary scattering matrix $\boldsymbol{S}$ (cf. Eq. (6)) and Fig. 4b, $-b_1(\lambda, 90°)/a_1(\lambda, 90°)$. Using Eq. (5), scaling the fluxes presented in Fig. 4a to obtain results for a Jupiter-like extrasolar planet in an arbitrary planetary system is a straightforward excercise. Note that P (Fig. 4b) is independent of the choice of r, R, d, D, and B_0, because P is a relative measure.

The flux and polarization spectra in Fig. 4 can be thought of to consist of a continuum with superimposed high-spectral resolution features that are due to absorption by CH_4. Recent Earth-based spectropolarimetric measurements of the gaseous planets of our own Solar System using ZIMPOL show a similar spectral structure (Joos et al. 2004).

For model 1, which is the clear atmosphere, the continuum F decreases steadily with λ (Fig. 4a), following the decrease of the molecular scattering optical thickness with λ. The continuum P (Fig. 4b) increases with λ, because the smaller the molecular optical thickness, the less multiple scattering takes place within the atmosphere; and multiple scattering tends to lower the degree of polarization of the reflected light. Multiple scattering also decreases with increasing absorption by CH_4. For model atmosphere 1, this fully explains the high values of P within the CH_4 absorption bands (Stam et al. 1999). In the strong absorption band around 0.89 μm, $P = 0.95$, and thus almost reaches its single scattering value at a single scattering angle of 90° (which corresponds with a planetary phase angle α of 90°), namely 0.96 (see Fig. 3b).

For model 2, which is the atmosphere with the tropospheric cloud, both F and P (Fig. 4a and 4b) at the shortest wavelengths are similar to those of model 1, because at these wavelengths, the molecular scattering optical thickness of the atmospheric layers above the cloud is so large that hardly any stellar light will reach the cloud layer. In the strong CH_4-absorption band around 0.89 μm, With increasing wavelength, the molecular scattering optical thickness decreases, and, at least at continuum wavelengths, the contribution of light scattered by the cloud particles to the reflected F and P increases. The slope of the continuum F is less steep for model 2 than for model 1, because while the molecular scattering optical thickness decreases with wavelength, the cloud's (scattering) optical thickness increases. The decrease of the continuum P for model 2 (Fig. 4b) is due to the increased multiple scattering within the cloud layers, as well as to the low degree of polarization of light that is scattered by cloud particles (see Fig. 3b).

In the CH_4-absorption bands, F is generally larger and P smaller for model 2 than for model 1, just like at continuum wavelengths. In the strong absorption band around 0.89 μm, however, F and P of the two models are similar, because at these wavelengths, hardly any stellar light can reach the cloud layer due to the large molecular absorption optical thickness of the atmosphere above the cloud. The light that is reflected at these wavelengths, has thus been scattered in the highest atmospheric layers, which are identical in model atmospheres 1 and 2.

For model 3, the atmosphere with the tropospheric cloud and the stratospheric haze, F is at all wavelengths somewhat larger than for model 2, even at the shortest wavelengths, where model 2 is almost indistinguishable from model 1 (Fig. 4a). The influence of the optically thin haze on F is explained by the relatively small molecular scattering and absorption optical thickness above the high-altitude haze layer: at all wavelengths, a significant fraction of the incoming stellar light reaches the haze layer and is reflected back to space. The degree of polarization P (Fig. 4b) for model 3 is at all wavelengths significantly lower than that for model 1 and 2 mainly because light that is singly scattered by the haze particles has a very low degree of polarization (see Fig. 3b). In particular, P is very low in the strong absorption band around 0.89 μm. Whereas in the

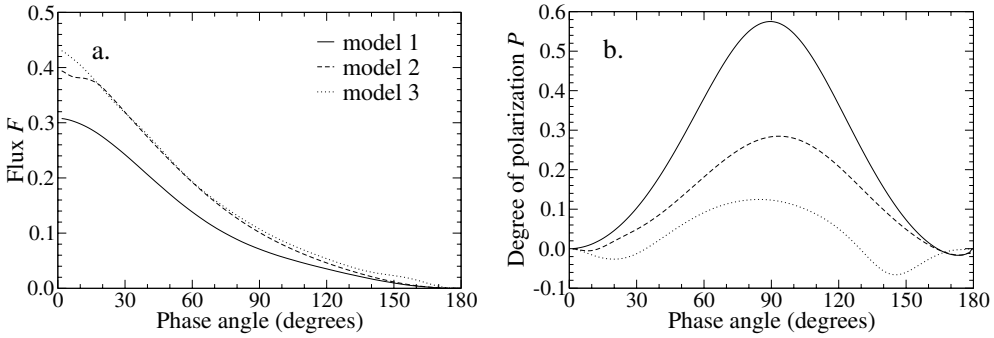

Fig. 5. The flux F and degree of polarization P of the reflected starlight for the three model atmospheres as functions of the planetary phase angle α, averaged over the wavelength region between 0.65 and 0.95 μm.

clear and cloudy atmospheres of models 1 and 2, the reflected light in this band has been scattered by molecules, in the atmosphere of model 3, the depolarizing haze particles are the main scatterers.

4.2. Flux and polarization as functions of phase angle

The flux and degree of polarization of reflected starlight not only depend on the planetary atmosphere, but also on the planetary phase angle α. As seen from the Earth, the gaseous planets of our own Solar System can only be observed at small phase angles (the maximum phase angle for Jupiter is, for example, about 11°, and for Saturn, 6°). The phase angles at which an extrasolar planet can be observed along its orbit range from $90° - i$ to $90° + i$, with i the orbital inclination angle ($i = 0°$ for an orbit that is viewed face-on). When $\alpha \approx 0°$ or $\alpha \approx 180°$, it will be impossible to spatially separate the extrasolar planet from its star and thus to measure F and/or P of the reflected starlight without including the direct stellar light, because in those cases the planet is located either behind or in front of the star. For completeness, we do include these phase angles in our calculations.

Figure 5 shows F (assuming $\pi B_0 r^2 R^2/(d^2 D^2)$ is equal to 1) and P for the three model atmospheres as functions of α, averaged over the wavelength region between 0.65 and 0.95 μm. We average over a wavelength region rather than present monochromatic results because due to the faintness of extrasolar planets, the first direct observations will probably be performed using broadband filters. We average over this particular wavelength region (the I-band) because that is where polarimetry with the CHEOPS instrument (Feldt et al. 2003) and ZIMPOL (Povel et al. 1990; Povel 1995) for the VLT (Feldt et al. 2003) is planned to take place.

The reflected flux in Fig. 5 equals $\frac{1}{4}a_1$, and thus, at $\alpha = 0°$ the planet's geometric albedo A_G (in this case averaged over the wavelength region between 0.65 and 0.95 μm). As can be seen in Fig. 5a, the reflected fluxes F are smooth functions of α. Only the curve for model atmosphere 2, with the tropospheric cloud layer, shows a slight depression at small phase angles. This depression can be attributed to the local minimum in the single scattering phase function of the cloud particles (see Fig. 3a) for scattering angles between 165° and 180°. Apart from the albedo, the reflected flux appears to be insensitive to the composition and structure of the model atmosphere.

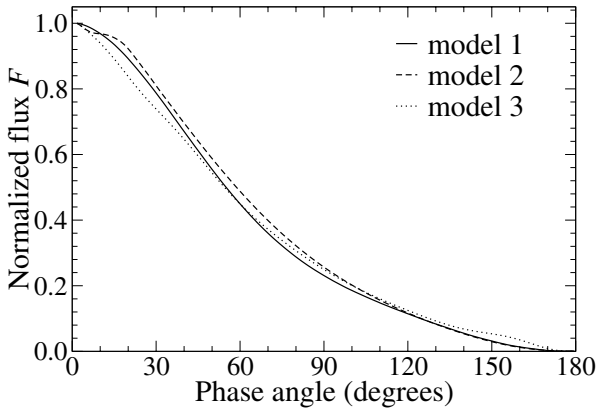

Fig. 6. The reflected flux F for the three model atmospheres as functions of α, averaged over the wavelength region between 0.65 and 0.95 μm, and normalized at $\alpha = 0°$.

This is illustrated in Fig. 6, where we have plotted the fluxes for the three model atmospheres normalized at $\alpha = 0°$, thus in fact, (see Eq. (8)) divided by the geometric albedo A_G For model atmosphere 1, we find $A_G = 0.31$, for model 2, $A_G = 0.39$, and for model 3, $A_G = 0.43$. From the curves in Fig. 6, we can conclude that without accurate information on $\pi B_0 r^2 R^2/(d^2 D^2)$ of an extrasolar planetary system, measuring F will yield little information about the atmosphere, even when the planet is observed at different phase angles.

The phase angle dependence of P depends strongly on the model atmosphere, except for reflection near the backward ($\alpha = 0°$) and forward ($\alpha = 180°$) directions, where P is zero regardless of the model atmosphere, because of symmetry principles. As explained before, such small and large phase angles will not be accessible for polarimetry of spatially resolved extrasolar planets anyway, because the planet will be either behind or in front of the star. From the Earth, the gaseous planets of our own Solar System are only observable at small phase angles. Earth-based polarimetry of these planets therefore always yields low values of P (see Joos et al. 2004 for recent Earth-based polarimetric measurements of Jupiter, Uranus and Neptune).

For all three model atmospheres in Fig. 5b, P peaks near $\alpha = 90°$, because P of the light that has been singly scattered by the gaseous molecules, which are present in each of the model atmospheres, is largest at a scattering angle of 90° (see

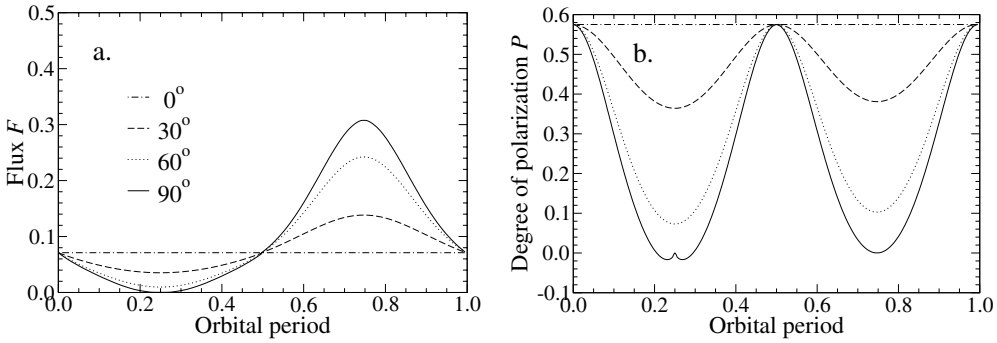

Fig. 7. The flux F and degree of polarization P of the reflected starlight averaged over the wavelength region between 0.65 and 0.95 μm, for model atmosphere 1 and different orbital inclination angles: 0° (dot-dashed line), 30° (dashed line), 60° (dotted line), and 90° (solid line).

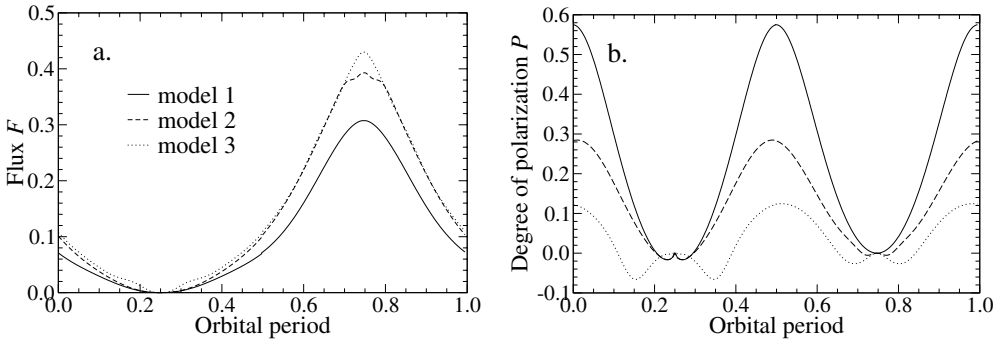

Fig. 8. The flux F and degree of polarization P of the reflected starlight averaged over the wavelength region between 0.65 and 0.95 μm, for an inclination angle of 90° and the three model atmospheres.

Fig. 3b). For models 1 and 2, $P > 0$ for phase angles smaller than about 165°, and the reflected starlight is thus polarized perpendicular to the planetary scattering plane. For larger phase angles (when only a narrow crescent of the planet is visible), $P < 0$ and the direction of polarization is thus parallel to the scattering plane. This negative polarization is characteristic for light that has been scattered twice by molecules in the planetary atmosphere. For these large phase angles, the contribution of the twice scattered light to P can be significant because the single scattered light is virtually unpolarized. For model 3, with the high altitude haze, $P < 0$ across a broader range of phase angles, because the haze particles themselves scatter negatively polarized light (see Fig. 3b).

4.3. Flux and polarization as functions of orbital period

As said before (in Sect. 4.2), the phase angles α an extrasolar planet can be observed at when it orbits its star range from $90° - i$ to $90° + i$ with i the orbital inclination angle. In Fig. 7, we have plotted F and P for the clear atmosphere (model 1) during an orbital period for various inclination angles and a circular orbit. Like before, $\pi B_0 r^2 R^2/(d^2 D^2)$ is assumed to equal 1.

Figure 7 shows that except when $i \approx 0°$ (when the orbit is seen face-on), F and P vary significantly during an orbital period: F is maximum when the planet's day-side is observed (at 0.75 orbital periods in Fig. 7) and zero when the planet's night-side is in view (at 0.25 orbital periods), while P peaks at 0.0 and 0.5 orbital periods, when $\alpha = 90°$. The polarization curve during the first half of the orbit (from 0.0 to 0.5) differs slightly from that during the second half (from 0.5 to 1.0), reflecting the asymmetry of the model 1 curve in Fig. 5b. When $i = 0°$, the observed fraction of the planet that is illuminated is constant, and F is thus constant. P's absolute value is also constant, but the direction of polarization, that will generally be perpendicular or parallel to the planetary scattering plane, can be seen to rotate with the planet as it orbits the star. The variation of P along the planetary orbit, either in absolute value or in direction, would help to distinguish the signal of the planet from possible background polarization signals, like that from zodiacal dust.

Interestingly, unlike the reflected stellar flux (Fig. 7a), the maximum degree of polarization that can be measured along the planetary orbit is independent of the orbital inclination angle (Fig. 7b). Because this maximum value does depend on the planetary atmosphere (see Fig. 5b), polarimetry could thus provide information about the planetary atmosphere without knowledge on the inclination angle.

The value of polarimetry along a planetary orbit for the characterization of EGPs is further illustrated in Fig. 8, which shows F and P along the planetary orbit for an inclination angle of 90° and the three model atmospheres. Because the inclination angle is 90°, all three polarization curves in Fig. 8b are zero at 0.25 and 0.75 orbital periods, when, respectively, the planet's night ($\alpha = 180°$) and dayside ($\alpha = 0°$) are turned towards the observer. Clearly, the maximum P of each curve depends strongly on the planetary atmosphere. Obviously, the

maximum value of F along the planetary orbit also depends on the planetary atmosphere (Fig. 8a). However, the maximum value of F will provide far less information on the planetary atmosphere than that of P, because 1) F's maximum depends on the orbital inclination angle; 2) F is less sensitive to the composition and structure of the planetary atmosphere; 3) F can be measured less accurately than P because P is a relative measure; and 4) to derive information on the planet from measured values of F, accurate knowledge about the planetary system (i.e. $\pi B_0 r^2 R^2/(d^2 D^2)$) is required.

5. Discussion and summary

In this paper, we present numerical simulations of the flux and degree of polarization of starlight that is reflected by Jupiter-like EGPs, to illustrate the advantages of polarimetry for the detection and characterization of such planets. The direct, unscattered (and unpolarized) starlight is not included in our simulations. Our simulations are thus representative of direct observations of extrasolar planets that orbit their star at Jupiter-like distances, with fluxes that can be observed spatially resolved from the stellar fluxes. Such observations may be carried out with e.g. adaptive optics systems on ground-based telescopes, such as CHEOPS (Feldt et al. 2003) that is planned for use on the VLT.

The main advantage of using polarimetry for the detection of extrasolar planets is that it can be used to distinguish the weak, polarized signal of starlight that is reflected by a planet from the strong, unpolarized, direct starlight. As such, polarimetry can be used for direct detections of planets that cannot be observed spatially resolved from their star (either because they are in a very close orbit, and/or because the star is too far away) (see Seager et al. 2000; Saar & Seager 2003; Hough & Lucas 2003), and for planets that can be spatially resolved. We concentrate on spatially resolvable Jupiter-like planets. Apart from their orbital distance, these planets differ from close-in giant planets in their atmospheric composition and structure, because far-out planets will generally be much cooler than planets close to their star.

Our simulations show that starlight that is reflected by Jupiter-like EGPs can have degrees of polarization of several tens of percent, thanks to the range of phase angles α at which EGPs will generally be observable from Earth (between $90^\circ - i$ and $90^\circ + i$, with i the orbital inclination angle). Only when $\alpha \approx 0^\circ$ or 180°, P will be close or equal to zero. At those phase angles, it will be very difficult to spatially resolve the planet from the star.

Because P is a relative measure, it can be determined with accuracies of the order of 10^{-5} (Povel 1995). Although such sensitivities are imperative for planet detection in unresolved planetary systems, the detection of a spatially resolvable EGP in a Jupiter-like orbit can be carried out with a less accurate polarimeter. However, the use of an accurate polarimeter is strongly recommended, because polarimetry is a valuable tool not only for detecting EGPs, but also for the characterization of their atmospheres, i.e. the derivation of chemical compositions, sizes, and spatial distributions of atmospheric constituents, such as cloud particles.

This application of polarimetry is illustrated by the sensitivity of P to the three model atmospheres in Figs. 4 and 5: both the degree of polarization in the continuum and across the gaseous absorption bands depend strongly on the atmospheric composition and structure. Because extrasolar planets are extremely faint, the spectral resolution of the first direct observations of extrasolar planets will probably be low, and would yield the continuum polarization. At short wavelengths, where the atmospheric molecular scattering optical thickness is large, the continuum polarization generally contains information on the upper atmospheric layers. At longer wavelengths, the atmospheric molecular scattering optical thickness is small, and the continuum polarization depends mainly on the scatterers in the deeper atmospheric layers, e.g. cloud particles. Across a gaseous absorption band, P contains information on particles at various altitudes in the atmosphere, and thus on the vertical structure of the atmosphere (Stam et al. 1999). Although the information content of P across gaseous absorption bands is very high, the spectral resolution that is required for such observations makes them extremely challenging for years to come.

Compared to flux observations, another advantage of polarimetry for the characterization of planetary atmospheres is that because P is a relative measure, it is independent of the distances between the planet and the star (D) and between the planet and the observer (d), the sizes of the planet (r) and the star (R), and the incoming stellar flux (B_0). So, when these parameters are not accurately known, as will often be the case with extrasolar planets, one can still derive atmospheric information from P (see Fig. 5b). Obtaining atmospheric information from reflected flux measurements appears to be a much harder task, because it requires an accurate measurement of the absolute flux, as can be concluded from Figs. 5a and 6.

Finally, because P is a relative measure, it is unaffected upon transmission through the Earth's atmosphere. The wavelength dependence of P, and in particular that across gaseous absorption bands, is thus retained without the need for atmospheric corrections. This advantage of polarimetry might be particularly valuable when searching for extrasolar planets with Earth-like atmospheres.

References

Burrows, A., Sudarsky, D., & Lunine, J. I. 2003, ApJ, 596, 587
Charbonneau, D., Brown, T. M., Latham, D. W., & Mayor, M. 2000, ApJ, 529, L45
Charbonneau, D., Brown, T. M., Noyes, R. W., & Gilliland, R. L. 2002, ApJ, 568, 377
De Haan, J. F., Bosma, P. B., & Hovenier, J. W. 1987, A&A, 183, 371
De Rooij, W. A., & van der Stap, C. C. A. H. 1984, A&A, 131, 237
Feldt, M., Turatto, M., Schmid, H. M., et al. 2003, In ESA SP–539, Towards Other Earths: DARWIN/TPF and the Search for Extrasolar Terrestrial Planets, ed. M. Fridlund, & Th. Henning, 99
Hansen, J. E., & Hovenier, J. W. 1974, J. Atmos. Sci., 31, 1137
Hansen, J. E., & Travis, L. D. 1974, Space Sci. Rev., 16, 527
Hough, J. H., & Lucas, P. W. 2003, In ESA SP–539, Towards Other Earths: DARWIN/TPF and the Search for Extrasolar Terrestrial Planets, ed. M. Fridlund, & Th. Henning, 11
Hovenier, J. W. 1969, J. Atmos. Sci., 26, 488

Hovenier, J. W., & van der Mee, C. V. M. 1983, A&A, 128, 1
Joos, F., Schmid, H. M., Gisler, D., et al. 2004, in Astronomical Polarimetry, ASP Conf. Ser., in press
Karkoschka, E. 1994, Icarus, 111, 174
Kemp, J. C., Henson, D., Steiner, C. T., & Powell, E. R. 1987, Nature, 326, 270
Lindal, G. F. 1992, ApJ, 103, 967
Marley, M. S., Gelino, C., Stephens, D., Lunine, J. I., & Freedman, R. 1999, ApJ, 513, 879
Martonchik, J. V., Orton, G. S., & Appleby, J. F. 1984, Appl. Opt., 23, 541
Mayor, M., & Queloz, D. 1995, Nature, 378, 355
Povel, H. P., Aebersold, H., & Stenflo, J. O. 1990, Appl. Opt., 29, 1186
Povel, H. P. 1995, Optical Engineering, 34, 1870
Saar, S. H., & Seager, S. 2003, In Scientific Frontiers in Research on Extrasolar Planets, ed. D. Deming, & S. Seager, ASP Conf. Ser., 294, 529
Seager, S., Whitney, B. A., & Sasselov, D. D. 2000, ApJ, 540, 504
Sromovsky, L. A., & Fry, P. M. 2002, Icarus, 157, 373
Stam, D. M., de Haan, J. F., Hovenier, J. W., & Stammes, P. 1999, J. Geophys. Res., 104, 16843
Van de Hulst, H. C. 1957, Light Scattering by Small Particles (New York: Wiley), also (New York: Dover), 1981
Vidal-Majar, A., Lecavelier des Etangs, A., Désert, J.-M., et al. 2003, Nature, 422, 143
Vidal-Majar, A., Désert, J.-M., Lecavelier des Etangs, A., et al. 2004, ApJ, 604, L69
West, R. A., Strobel, D. F., & Tomasko, M. G. 1986, Icarus, 65, 161